References and Notes

1. E. I. Solomon, U. M. Sundaram, T. E. Machonkin, *Chem. Rev.* **96**, 2563 (1996).
2. H. Decker, R. Dillinger, F. Tuczek, *Angew. Chem. Int. Ed. Engl.* **39**, 1591 (2000).
3. S. Mandal, D. Macikenas, J. D. Protasiewicz, L. M. Sayre, *J. Org. Chem.* **65**, 4804 (2000).
4. L. M. Mirica, X. Ottenwaelder, T. D. P. Stack, *Chem. Rev.* **104**, 1013 (2004).
5. E. A. Lewis, W. B. Tolman, *Chem. Rev.* **104**, 1047 (2004).
6. L. Santagostini *et al.*, *Chem. Eur. J.* **6**, 519 (2000).
7. S. Itoh *et al.*, *J. Am. Chem. Soc.* **123**, 6708 (2001).
8. L. M. Mirica *et al.*, *J. Am. Chem. Soc.* **124**, 9332 (2002).
9. M. Kim *et al.*, *Nat. Struct. Biol.* **9**, 591 (2002).
10. J. C. Price, E. W. Barr, B. Tirupati, J. M. Bollinger, C. Krebs, *Biochemistry* **42**, 7497 (2003).
11. M. T. Green, J. H. Dawson, H. B. Gray, *Science* **304**, 1653 (2004).
12. Note that a synthetic μ-η^2:η^2-peroxodicopper(II) complex has been shown to directly hydroxylate an aromatic ring on a noncoordinating substrate (*32*).
13. A lower yield of the products is observed for electron-deficient substrates.
14. Materials and methods are available as supporting material on *Science* Online.
15. Both catechol and quinone are produced upon acidic workup of the solution mixture, which supports **A** as a reactive species during hydroxylation.
16. J. A. Halfen *et al.*, *Science* **271**, 1397 (1996).
17. S. Mahapatra, V. G. Young, S. Kaderli, A. D. Zuberbühler, W. B. Tolman, *Angew. Chem. Int. Ed. Engl.* **36**, 130 (1997).
18. V. Mahadevan *et al.*, *J. Am. Chem. Soc.* **119**, 11996 (1997).
19. A resonance Raman spectrum resulting from 600-nm excitation shows a C–O stretch at 1280 cm^{-1}, which supports a phenolate to Cu charge-transfer assignment.
20. M. J. Henson, P. Mukherjee, D. E. Root, T. D. P. Stack, E. I. Solomon, *J. Am. Chem. Soc.* **121**, 10332 (1999).
21. No vibrations characteristic for **P** complexes (at ~300 or ~730 cm^{-1}) are observed.
22. S. Yamazaki, S. Itoh, *J. Am. Chem. Soc.* **125**, 13034 (2003).
23. J. L. DuBois *et al.*, *J. Am. Chem. Soc.* **119**, 8578 (1997).
24. J. L. DuBois *et al.*, *J. Am. Chem. Soc.* **122**, 5775 (2000).
25. EXAFS analysis typically cannot distinguish between atoms that differ in Z by 1 (e.g., O and N) (*33*). Given the k range of the EXAFS data (k = 3 to 12.5 $Å^{-1}$), any difference in R less than 0.17 Å between ligands in the first coordination shell (at 1.89 Å) could not be resolved.
26. V. Mahadevan, M. J. Henson, E. I. Solomon, T. D. P. Stack, *J. Am. Chem. Soc.* **122**, 10249 (2000).
27. An electrophilic aromatic substitution mechanism for a bis-μ-oxodicopper(III) complex has been proposed in a case in which a ligand aryl group is hydroxylated (*34*).
28. P. Chen, E. I. Solomon, *J. Inorg. Biochem.* **88**, 368 (2002).
29. E. I. Solomon, P. Chen, M. Metz, S.-K. Lee, A. E. Palmer, *Angew. Chem. Int. Ed. Engl.* **40**, 4570 (2001).
30. D. E. Wilcox *et al.*, *J. Am. Chem. Soc.* **107**, 4015 (1985).
31. P. E. M. Siegbahn, *J. Biol. Inorg. Chem.* **8**, 567 (2003).
32. E. Pidcock, H. V. Obias, C. X. Zhang, K. D. Karlin, E. I. Solomon, *J. Am. Chem. Soc.* **120**, 7841 (1998).
33. R. A. Scott, *Methods Enzymol.* **117**, 414 (1985).
34. P. L. Holland, K. R. Rodgers, W. B. Tolman, *Angew. Chem. Int. Ed. Engl.* **38**, 1139 (1999).

35. We thank R. Pratt for assistance in the synthesis of ^{18}O-di-*t*-butyl-phenolate and J. I. Brauman for insightful discussions. L.M.M. gratefully acknowledges a John Stauffer Stanford Graduate Fellowship. Funding was provided by NIH GM50730 (T.D.P.S), NIH DK31450 (E.I.S.), and NIH RR01209 (K.O.H.). XAS data were measured at the Stanford Synchrotron Radiation Laboratory (SSRL), which is supported by the Department of Energy, Office of Basic Energy Sciences. The SSRL Structural Molecular Biology program is funded by the National Institutes of Health, National Center for Research Resources, Biomedical Technology Program, and the Department of Energy, Office of Biological and Environmental Research.

Supporting Online Material

www.sciencemag.org/cgi/content/full/308/5730/1890/DC1
Materials and Methods
SOM Text
Figs. S1 to S8
Tables S1 to S3
References

10 March 2005; accepted 10 May 2005
10.1126/science.1112081

Sound Velocities of Hot Dense Iron: Birch's Law Revisited

Jung-Fu Lin,[1]* Wolfgang Sturhahn,[2] Jiyong Zhao,[2] Guoyin Shen,[3] Ho-kwang Mao,[1] Russell J. Hemley[1]

Sound velocities of hexagonal close-packed iron (hcp-Fe) were measured at pressures up to 73 gigapascals and at temperatures up to 1700 kelvin with nuclear inelastic x-ray scattering in a laser-heated diamond anvil cell. The compressional-wave velocities (V_P) and shear-wave velocities (V_S) of hcp-Fe decreased significantly with increasing temperature under moderately high pressures. V_P and V_S under high pressures and temperatures thus cannot be fitted to a linear relation, Birch's law, which has been used to extrapolate measured sound velocities to densities of iron in Earth's interior. This result means that there are more light elements in Earth's core than have been inferred from linear extrapolation at room temperature.

The properties of Earth's iron-rich core have been inferred from estimates of iron density at high pressures and temperatures and from measurements of compressional-wave (V_P) and shear-wave (V_S) velocities passing through the core (*1*–*13*). These data have indicated that Earth's core is less dense than pure iron by approximately 10% for the outer core and 3% for the inner core, suggesting the existence of light elements in the core. On the other hand, Birch's law, a linear sound velocity–density relation (*2*, *14*, *15*), has also been used to extrapolate measured sound velocities at high pressures and room temperatures to inner core conditions without considering the temperature effect (*9*, *12*). This linear extrapolation has suggested that the inner core is mainly made of Fe-Ni alloy. The nuclear-resonant inelastic x-ray scattering (NRIXS) technique provides a direct probe of the phonon density of states (DOS) of the resonant isotope (*16*–*18*) using the 14.4125-keV transition of ^{57}Fe. V_P and V_S of hexagonal close-packed (hcp) Fe have been measured up to 153 GPa at 300 K (*10*, *19*). However, the effect of temperature on the sound velocity measurements of Fe in static studies is not well understood. Here we report the static NRIXS study of the sound velocities of hcp-Fe up to 73 GPa and 1700 K in a laser-heated diamond anvil cell (LHDAC), and we discuss the temperature effect on the sound velocities and Birch's law.

We conducted NRIXS experiments in an LHDAC at Sector 3 of the Advanced Photon Source (APS) at Argonne National Laboratory (*20*, *21*). Energy spectra were obtained by tuning the x-ray energy (±70 meV) around the nuclear transition energy of 14.4125 keV and collecting the Fe K-fluorescence (the emission of an x-ray photon via the transition of an atomic electron into an unoccupied 1s state) radiation that was emitted with time delay relative to the incident x-ray pulses. We used a quasiharmonic model to extract the phonon DOS from the NRIXS spectra (Fig. 1) according to the procedure described in (*16*–*18*). With the NRIXS technique, we measured the spectrum of the self-correlation function of the position of the Fe atoms (*17*). In the model, the atomic motions relative to the temperature-dependent averaged position are assumed to be harmonic under the given conditions of pressure, temperature, and other parameters. Thermal effects, such as expansion and change of force constants with atomic distances, were allowed to change but the vibrations were still assumed to occur in a harmonic potential. The average kinetic energy and force constant independently derived from the moments of the measured spectra were consistent with the values evaluated from the quasiharmonic model (*17*), indicating the validity of the model to our high-pressure/temperature data (*22*). The Debye sound velocity (V_D) was derived from parabolic fitting of the low-energy regime of the DOS (*16*–*18*), and the vibrational, elastic, and thermodynamic parameters were obtained by the integration of the DOS. We then calculated the thermal

[1]Geophysical Laboratory, Carnegie Institution of Washington, 5251 Broad Branch Road, N.W., Washington, DC 20015, USA. [2]Advanced Photon Source, Argonne National Laboratory, 9700 South Cass Avenue, Argonne, IL 60439, USA. [3]Consortium for Advanced Radiation Sources, The University of Chicago, Chicago, IL 60637, USA.

*To whom correspondence should be addressed. E-mail: j.lin@gl.ciw.edu

equation-of-state (EOS) parameters of hcp-Fe using the thermal EOS from previous studies (*23*–*25*) and the Birch-Murnaghan EOS (*26*). The adiabatic bulk modulus at zero pressure (K_{0S}) is

$$K_{0S}(T) = K_{0T}(T)(1 + \alpha\gamma T) \quad (1)$$

where K_{0T} is the isothermal bulk modulus at zero pressure (*23*), α is the thermal expansion coefficient (*23*), γ is the Grüneisen parameter (γ = 1.78) (*25*), and T is the temperature. The Birch-Murnaghan EOS is used to calculate the isothermal bulk modulus at high pressures (K_T) and the adiabatic bulk modulus at high pressures (K_S). The K_S, density (ρ), and V_D are used to solve for the aggregate V_P, V_S, and shear modulus G by the following equations (*10*)

$$\frac{K_S}{\rho} = V_P^2 - \frac{4}{3}V_S^2 = V_\Phi{}^2 \quad (2)$$

$$\frac{G}{\rho} = V_S^2 \quad (3)$$

$$\frac{3}{V_D^3} = \frac{1}{V_P^3} + \frac{2}{V_S^3} \quad (4)$$

where V_ϕ is the bulk sound velocity calculated from the thermal EOS parameters of K_S and ρ. The derivation of V_S is relatively insensitive to the differences in the EOS data (*27*). Our results at high pressures and room temperatures are consistent with those of a previous study (*10*). At high temperatures, the bulk sound velocity (V_ϕ) followed Birch's law (V_ϕ is linearly related to the density and mean atomic weight; $dV_\phi/dT = 0$) (*14*), whereas V_P, V_S, and G did not (Fig. 2). At a pressure of ~54 GPa, V_P decreased by ~7%, V_S decreased by ~14%, and G decreased by ~28%, with a temperature increase of 1000 K. The effect of temperature on the sound velocities at constant density is smaller than the effect at constant pressure; i.e., at a density of ~10.25 g cm^{-3}, V_P decreased at a rate of 0.00035 km s^{-1} K^{-1} (dV_P/dT), V_S decreased by 0.00046 km s^{-1} K^{-1} (dV_S/dT), and G decreased by 0.035 GPa K^{-1} (dG/dT). These values are in general agreement with the V_ϕ-density linear relation; if V_ϕ is linearly related to the density without temperature effect, then $V_P(dV_P/dT) - 4/3V_S(dV_S/dT) = 0$ (from Eq. 2). X-ray diffraction spectra showed that the samples after laser heating were in the polycrystalline hcp structure at high pressures without significant preferred orientation, suggesting that the strong effect of temperature on the sound velocities cannot be explained simply by the elastic anisotropy in highly textured hcp-Fe, which can account for a few percent of the difference in V_P (*12*). Different thermal pressure conditions varying from no thermal pressure effect to full thermal pressure effect (*28*) have been used to test the systematic errors in the temperature effect on the sound velocities. We found that the uncertainties in the thermal pressure alone were too small to result in a significant temperature effect on the sound velocities, in particular, the temperature effect on V_S.

Extrapolated sound velocities of hcp-Fe at 3000 and 6000 K, obtained by combining our study at moderate pressure and temperature with a previous NRIXS study at high pressures and 300 K and with shock-wave data at high pressure and high temperature, show that the effect of temperature on the sound velocities of Fe is significant at moderate pressures, but weakens under inner core pressures because a highly compressed Fe has a smaller thermal

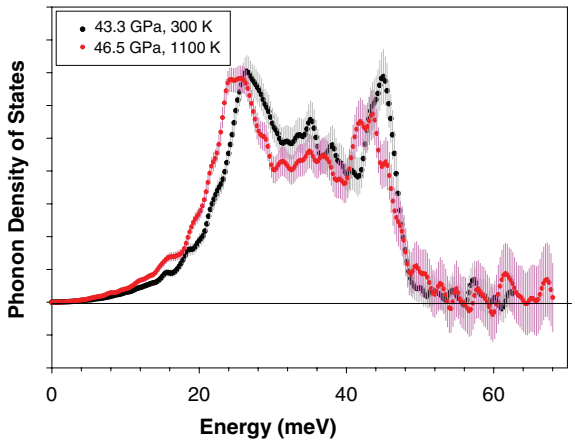

Fig. 1. DOS of hcp-Fe at 43.3 (±2.2) GPa and 300 K (black curve) and 46.5 (±2.8) GPa and 1100 K (±100) (red curve). The spectral features of the DOS are shifted toward lower energies and the initial slope of the low-energy regime increases significantly at high temperature, indicating the softening of the lattice excitation. Debye sound velocities are derived from parabolic fitting of the low-energy regime of the DOS in the range of 3.5 to 14 meV.

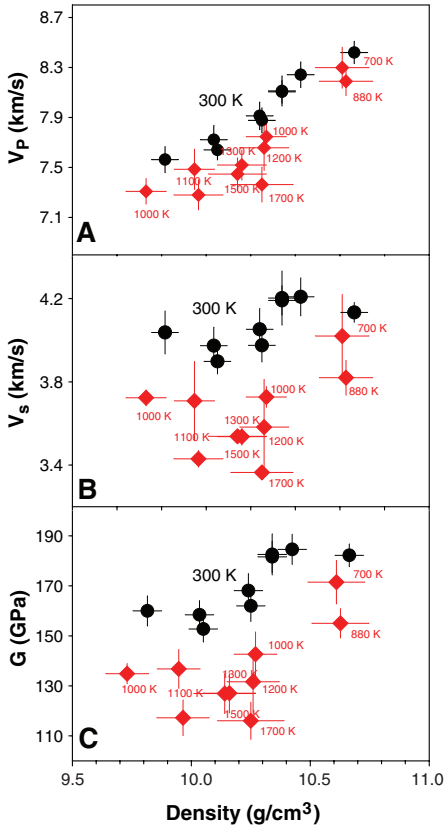

Fig. 2. Experimental results of aggregate V_P (**A**), V_S (**B**), and G (**C**) of hcp-Fe at high pressures and temperatures. Black circles, 300 K; red diamonds, high temperatures. Temperatures are given next to the red diamonds.

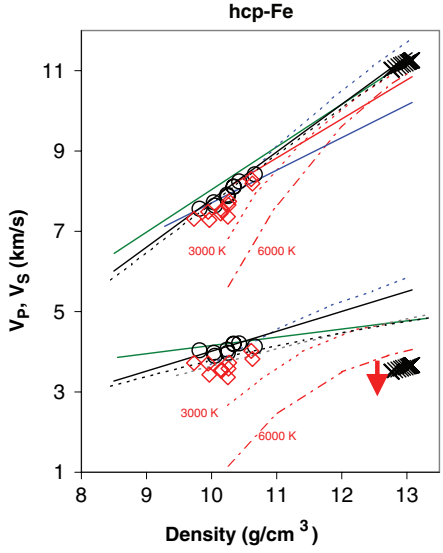

Fig. 3. Comparison of V_P and V_S of hcp-Fe at high pressures and temperatures. Black open circles, this study at 300 K; red open diamonds, this study at high temperatures; X's, Preliminary Earth Reference Model (PREM) (*29*); red solid line, shock wave (*3*); blue dashed line, radial x-ray diffraction at 300 K (*6*); black solid line, NRIXS at 300 K (*10*); black dashed line, x-ray diffraction to 300 GPa and 1200 K (*30*); blue solid line, IXS at 300 K (*9*); green solid line, IXS at 300 K (*12*); gray dashed line, x-ray diffraction study up to 330 GPa and 300 K (*31*); red dashed line (3000 K) and red dash-dotted line (6000 K), extrapolated sound velocities of hcp-Fe at 3000 and 6000 K. At a density of ~10.25 g cm^{-3}, we used the slope of 0.00035 km s^{-1} K^{-1} to extrapolate V_P and 0.00046 km s^{-1} K^{-1} to extrapolate V_S. At higher pressures, we used a previous NRIXS study at high pressures and 300 K (*10*) and shock-wave data at high pressure and high temperature (*3*) to calculate V_P and V_S at 3000 and 6000 K. The red arrow indicates that the extrapolated shear wave of hcp-Fe in the inner core should be further corrected downward, to lower values.

expansion (Fig. 3) (*3*, *9*, *10*, *12*, *29–31*). Because the temperature of the inner core is believed to be close to the melting curve of Fe, the extrapolated V_S of hcp-Fe in the inner core should be corrected to even lower values. The small deviation in V_P between shock-wave data (*3*) and the previous NRIXS study (*10*) at high pressures and room temperature also suggests that the temperature effect on V_P is suppressed under inner core conditions, whereas the large difference in the V_S indicates that temperature has a strong effect on V_S even under core pressures (Fig. 3). Theoretical calculations on the elasticity of hcp-Fe predicted that V_S and G would decrease with increasing temperature at a constant density of 13.04 g cm^{-3} (*11*).

Birch pointed out the likely temperature effect on the sound velocities in his original paper in 1961 (*2*). Our results confirm this idea. It has been shown that the addition of a light element such as Si or S into Fe increases V_P and V_S under high pressures (*32*, *33*). Considering the temperature effect on V_P and V_S of hcp-Fe at inner core pressures and 6000 K (*20*), a few percent of light elements alloyed with Fe are still needed in the inner core to increase V_P to match seismic models (Fig. 3). This results in more light elements in Earth's inner core than has been suggested from the linearly extrapolated V_P of hcp-Fe at high pressures and room temperature (*12*).

References and Notes

1. F. Birch, *J. Geophys. Res.* **57**, 227 (1952).
2. F. Birch, *Geophys. J. R. Astron. Soc.* **4**, 295 (1961).
3. J. M. Brown, R. G. McQueen, *J. Geophys. Res.* **91**, 7485 (1986).
4. J. D. Bass, B. Svendsen, T. J. Ahrens, in *High Pressure Research in Mineral Physics*, M. H. Manghnani, Y. Syono, Eds. (American Geophysical Union, Washington, DC, 1987), pp. 393–423.
5. H. K. Mao, Y. Wu, L. C. Chen, J. F. Shu, *J. Geophys. Res.* **95**, 21737 (1990).
6. H. K. Mao *et al.*, *Nature* **396**, 741 (1999).
7. G. Steinle-Neumnn, L. Stixrude, R. E. Cohen, *Phys. Rev. B* **60**, 791 (1999).
8. D. Alfe, M. J. Gillan, G. D. Price, *Nature* **405**, 172 11 (2000).
9. G. Fiquet, J. Badro, F. Guyot, H. Requardt, M. Krisch, *Science* **291**, 468 (2001).
10. H. K. Mao *et al.*, *Science* **292**, 914 (2001).
11. G. Steinle-Neumann, L. Stixrude, R. E. Cohen, *Nature* **413**, 57 (2001).
12. D. Antonangeli *et al.*, *Earth Planet. Sci. Lett.* **225**, 243 (2004).
13. J. H. Nguyen, N. C. Holmes, *Nature* **306**, 2239 (2004).
14. R. C. Liebermann, A. E. Ringwood, *J. Geophys. Res.* **78**, 6926 (1973).
15. A. J. Campbell, D. L. Heinz, *Science* **257**, 66 (1992).
16. W. Sturhahn *et al.*, *Phys. Rev. Lett.* **74**, 3832 (1995).
17. W. Sturhahn, V. G. Kohn, *Hyperfine Interactions* **123/124**, 367 (1999).
18. M. Hu *et al.*, *Phys. Rev. B* **67**, 094304 (2003).
19. R. Lübbers, H. F. Grünsteudel, A. I. Chumakov, G. Wortmann, *Science* **287**, 1250 (2000).
20. Materials and methods are available as supporting material on *Science* Online.
21. J. F. Lin *et al.*, *Geophys. Res. Lett.* **31**, L14611 (2004).
22. G. Shen *et al.*, *Phys. Chem. Miner.* **31**, 353 (2004).
23. L. S. Dubrovinsky, S. K. Saxena, P. Lazor, *Phys. Chem. Miner.* **25**, 434 (1998).
24. L. S. Dubrovinsky, S. K. Saxena, F. Tutti, S. Rekhi, *Phys. Rev. Lett.* **84**, 1720 (2000).
25. L. S. Dubrovinsky, S. K. Saxena, N. A. Dubrovinskais, S. Rekhi, T. LeBihan, *Am. Mineral.* **85**, 386 (2000).
26. F. Birch, *J. Geophys. Res.* **83**, 1257 (1978).
27. W. Mao *et al.*, *Geophys. Res. Lett.* **31**, L15618 (2004).
28. D. L. Heinz, *Geophys. Res. Lett.* **17**, 1161 (1990).
29. A. M. Dziewonski, D. L. Anderson, *Phys. Earth Planet. Inter.* **25**, 297 (1981).
30. L. S. Dubrovinsky, N. A. Dubrovinskais, T. LeBihan, *Proc. Natl. Acad. Sci. U.S.A.* **98**, 9484 (2001).
31. O. L. Anderson, L. S. Dubrovinsky, S. K. Saxena, T. LeBihan, *Geophys. Res. Lett.* **28**, 399 (2001).
32. J. F. Lin *et al.*, *Geophys. Res. Lett.* **30**, 2112 (2003).
33. J. F. Lin *et al.*, *Earth Planet. Sci. Lett.* **226**, 33 (2004).

34. This work and use of the APS are supported by the U.S. Department of Energy (DOE), Basic Energy Sciences (BES), Office of Science, under contract no. W-31-109-ENG-38, and by the state of Illinois under the Higher Education Cooperation Act. We thank GeoSoilEnviroCARS and APS for the use of the ruby fluorescence system and E. E. Alp, D. Errandonea, S.-K. Lee, V. Struzhkin, M. Hu, D. L. Heinz, G. Steinle-Neumann, R. Cohen, J. Burke, V. Prakapenka, M. Rivers, S. Hardy, T. Duffy, and J. M. Jackson for their help and discussions. Work at Carnegie was supported by DOE/BES, DOE/National Nuclear Security Administration (Carnegie/DOE Alliance Center), NSF, and the W. M. Keck Foundation.

Supporting Online Material

www.sciencemag.org/cgi/content/full/308/5730/1892/DC1
Materials and Methods
Fig. S1
Table S1
References

2 March 2005; accepted 17 May 2005
10.1126/science.1111724

Deep-Sea Temperature and Circulation Changes at the Paleocene-Eocene Thermal Maximum

Aradhna Tripati* and Henry Elderfield

A rapid increase in greenhouse gas levels is thought to have fueled global warming at the Paleocene-Eocene Thermal Maximum (PETM). Foraminiferal magnesium/calcium ratios indicate that bottom waters warmed by 4° to 5°C, similar to tropical and subtropical surface ocean waters, implying no amplification of warming in high-latitude regions of deep-water formation under ice-free conditions. Intermediate waters warmed before the carbon isotope excursion, in association with downwelling in the North Pacific and reduced Southern Ocean convection, supporting changing circulation as the trigger for methane hydrate release. A switch to deep convection in the North Pacific at the PETM onset could have amplified and sustained warming.

PETM was a short-lived global warming event about 55 million years ago (Ma) that may provide insights into the environmental consequences of rising greenhouse gas levels (*1*, *2*). A reduction in the carbonate content of deep-sea sediments (*2*) and a large negative excursion in marine and terrestrial carbon isotope ($\delta^{13}C$) records (*1–3*) are associated with the PETM and indicate the addition of ^{13}C-depleted carbon to the oceans and atmosphere. A possible source of this carbon was the dissociation of ~1000 to 2100 gigatons (Gt) of methane hydrate in ocean sediments (*4*), most or all of which would have oxidized, raising atmospheric CO_2 by 70 to 160 parts per million by volume (ppmv) (*5*, *6*). Benthic foraminiferal taxa exhibit increased extinction rates during the PETM, probably because of deep-sea oxygen deficiency and a decrease in seawater carbonate ion concentration (*2*).

The climatic response to rising greenhouse gas levels in the past has been debated because of equivocal ocean temperature reconstructions based on foraminiferal oxygen isotope ratios ($\delta^{18}O_C$), which are a function of both temperature and seawater $\delta^{18}O$ ($\delta^{18}O_W$). To circumvent this ambiguity, the Mg/Ca temperature proxy has been applied to planktonic foraminifera, and it documented a 4 to 5°C warming of sea-surface temperatures (SST) across the PETM in the subtropical (*7*) and tropical ocean (*7*, *8*).

We investigated the evolution of deep-sea temperatures, high-latitude SST, and circulation patterns using foraminiferal Mg/Ca and stable isotope ratios (*9*, *10*) in order to examine the causes and consequences of the $\delta^{13}C$ excursion and the PETM. We used Mg/Ca ratios of benthic foraminifera to develop estimates of bottom water temperatures (T_B) for deep sites in the subtropical South Atlantic (Site 527) and tropical North Pacific (Site 1209) oceans, and for a site at intermediate depths in the equatorial Pacific Ocean (Site 865) (table S1). These temperatures should reflect surface conditions in high-latitude regions of deep-water formation. We integrated these data with SST records (*7*, *8*) to study the spatial pattern of warming and changes in the

Department of Earth Sciences, University of Cambridge, Downing Street, CB2 3EQ, UK.

*To whom correspondence should be addressed. E-mail: atri02@esc.cam.ac.uk